

Numerical computation of travelling breathers in Klein-Gordon chains

Yannick SIRE*, Guillaume JAMES

Mathématiques pour l'Industrie et la Physique, UMR CNRS 5640

Département GMM, Institut National des Sciences Appliquées,
135 avenue de Rangueil, 31077 Toulouse Cedex 4, France.

e-mail : sire@insa-toulouse.fr, james@insa-toulouse.fr

October 2004

Abstract

We numerically study the existence of travelling breathers in Klein-Gordon chains, which consist of one-dimensional networks of nonlinear oscillators in an anharmonic on-site potential, linearly coupled to their nearest neighbors. Travelling breathers are spatially localized solutions having the property of being exactly translated by p sites along the chain after a fixed propagation time T (these solutions generalize the concept of solitary waves for which $p = 1$). In the case of even on-site potentials, the existence of small amplitude travelling breathers superposed on a small oscillatory tail has been proved recently (G. James and Y. Sire, to appear in *Comm. Math. Phys.*, 2004), the tail being exponentially small with respect to the central oscillation size. In this paper we compute these solutions numerically and continue them into the large amplitude regime for different types of even potentials. We find that Klein-Gordon chains can support highly localized travelling breather solutions superposed on an oscillatory tail. We provide examples where the tail can be made very small and is difficult to detect at the scale of central oscillations. In addition we numerically observe the existence of these solutions in the case of non even potentials.

Keywords: travelling breathers; nonlinear lattices; numerical continuation, center manifold reduction.

*Corresponding author

1 Introduction

We consider a chain of nonlinear oscillators described by the following system (discrete Klein-Gordon equation)

$$\frac{d^2 x_n}{d\tau^2} + V'(x_n) = \gamma(x_{n+1} + x_{n-1} - 2x_n), \quad n \in \mathbb{Z}. \quad (1)$$

System (1) describes an infinite chain of particles linearly coupled to their nearest neighbors, in the local potential V . We denote by x_n the displacement of the n th particle from an equilibrium position, $V(x)$ a smooth anharmonic on-site potential satisfying $V'(0) = 0$, $V''(0) = 1$, and $\gamma > 0$ the coupling constant. This class of systems has been used in particular as a prototype for analyzing the effects of nonlinearity and spatial discreteness on localization of vibrational energy and energy transport (see [21] for a review). Equation (1) yields in particular the Peyrard-Bishop model for DNA denaturation [35, 12] if one chooses V as a Morse potential.

This paper deals with solutions of (1) satisfying

$$x_n(\tau) = x_{n-p}(\tau - T), \quad (2)$$

for a fixed integer $p \geq 1$ (p being the smallest possible) and $T \in \mathbb{R}$. The case when $p = 1$ in (2) corresponds to travelling waves with velocity $1/T$. Solutions satisfying (2) for $p \neq 1$ consist of pulsating travelling waves, which are exactly translated by p sites after a fixed propagation time T and are allowed to oscillate as they propagate on the lattice. Solutions of type (2) having the additional property of spatial localization ($x_n(\tau) \rightarrow 0$ as $n \rightarrow \pm\infty$) are known as *exact* travelling breathers (with velocity p/T) for $p \geq 2$ and solitary waves for $p = 1$.

Approximate travelling breather solutions (i.e. spatially localized solutions satisfying (2) only approximately) have been extensively studied. These solutions have been numerically observed in various one-dimensional nonlinear lattices such as Klein-Gordon chains [13, 46, 9, 5, 11], Fermi-Pasta-Ulam lattices [44, 7, 37, 19] and the discrete nonlinear Schrödinger (DNLS) equation [18, 15] (see [21] for more references). These solutions have been studied also in more sophisticated nonlinear models describing energy transport in alpha-helix [23, 39] and DNA [22]. One way of generating approximate travelling breathers consists of “kicking” static breathers consisting of spatially localized and time periodic oscillations (see the basic paper [31] for more details on these solutions). Static breathers are put into motion by perturbation in the direction of a pinning mode [9, 5]. The possible existence of an energy barrier (“Peierls-Nabarro barrier”) that the breather has to overcome in order to become mobile has drawn a lot of attention, see e.g. [13, 5, 19, 29] and the review paper [40]. An analytical method recently developed by MacKay and Sepulchre [32] allows to approximate the nonuniform

breather motion along the chain (the breather center approximately moves under the action of an effective potential). An application to the Fermi-Pasta-Ulam lattice can be found in [29].

In the small amplitude regime, spatially localized solutions of (1)-(2) have been studied analytically by Iooss and Kirchgässner [25] for $p = 1$ (case of travelling waves). Travelling wave solutions of (1) have the form $x_n(\tau) = x_0(\tau - nT)$ and are determined by the scalar advance-delay differential equation

$$\frac{d^2 x_0}{d\tau^2} + V'(x_0) = \gamma (x_0(\tau + T) - 2x_0 + x_0(\tau - T)). \quad (3)$$

Extension to larger values of p has been performed by James and Sire [41, 28, 42] (case of pulsating travelling waves). For fixed $p \geq 1$, problem (1)-(2) reduces to the p -dimensional system of advance-delay differential equations

$$\frac{d^2}{d\tau^2} \begin{bmatrix} x_1 \\ \vdots \\ x_n \\ \vdots \\ x_p \end{bmatrix} + \begin{bmatrix} V'(x_1) \\ \vdots \\ V'(x_n) \\ \vdots \\ V'(x_p) \end{bmatrix} = \gamma \begin{bmatrix} x_2(\tau) - 2x_1(\tau) + x_p(\tau + T) \\ \vdots \\ x_{n+1}(\tau) - 2x_n(\tau) + x_{n-1}(\tau) \\ \vdots \\ x_1(\tau - T) - 2x_p(\tau) + x_{p-1}(\tau) \end{bmatrix}. \quad (4)$$

System (4) is analyzed in the above references using a center manifold reduction in the infinite dimensional case, as described e.g. in reference [47]. It is rewritten as a reversible evolution problem in a suitable functional space, and considered for parameter values (T, γ) near critical curves where the imaginary part of the spectrum of the linearized operator consists of a pair of double eigenvalues and pairs of simple ones (the number of pairs is finite and equals the number of resonant phonons). Close to these curves, the pair of double eigenvalues splits into two pairs of hyperbolic eigenvalues with opposite nonzero real parts, which opens the possibility of finding solutions homoclinic to 0. Near these parameter values, the center manifold theorem reduces the problem locally to a reversible finite dimensional system of differential equations. The reduced system is put in a normal form which is integrable up to higher order terms. In some regions of the parameter space, the *truncated* normal form admits reversible orbits homoclinic to 0, which bifurcate from the trivial state and correspond to approximate solutions of (4).

Exact small amplitude solutions of (1)-(2) close to these approximate solutions (in a sense that we shall specify, allowing the existence of a small oscillatory tail) have been obtained for $p = 1$ [25], and for $p = 2$ in the case of even potentials V [28]. In both cases, the simplest homoclinic bifurcation yields a 6-dimensional reversible reduced system. As it is shown by Lombardi for different classes of reversible systems having a slow hyperbolic part and fast oscillatory modes [30]

(see also [8] for related numerics), reversible solutions of the truncated normal form homoclinic to 0 should not *generically* persist when higher order terms are taken into account in the normal form. The existence of corresponding travelling waves ($p = 1$) or travelling breathers ($p = 2$) decaying exactly to 0 should be a codimension-1 phenomenon, the codimension depending on the number of pairs of simple purely imaginary eigenvalues in the considered parameter regime (there is one pair of purely imaginary eigenvalues, in addition to hyperbolic ones). However, to confirm the nonexistence of reversible orbits homoclinic to 0 (close to a small amplitude homoclinic orbit of the truncated normal form) *for a given choice of V , γ , T* , one has to check the nonvanishing of a certain Melnikov function being extremely difficult to compute in practice [30]. Due to this codimension-1 character, in a given system (4) (with $p = 1$, or $p = 2$ and V even), γ and V being fixed, exact travelling wave or travelling breather solutions decaying to 0 at infinity might exist in the small amplitude regime, but for isolated values of the velocity p/T (see [20] for examples of nonlinear lattices supporting explicit travelling breather solutions with particular velocities).

Instead of orbits homoclinic to 0, the full normal form admits orbits homoclinic to small periodic ones [30] (originating from the pair of purely imaginary eigenvalues). These solutions correspond to exact solitary wave ($p = 1$) or travelling breather ($p = 2$) solutions of (1) superposed on a small periodic oscillatory tail, which can be made exponentially small with respect to the central oscillation size (the minimal tail size should be *generically* nonzero for a given value of (T, γ)). This phenomenon is in accordance with numerical observations in the case of travelling waves [5], and should explain numerical convergence problems arising in the computation of fully localized solitary waves or travelling breathers in various nonlinear lattices [43, 3].

For asymmetric potentials V and $p \geq 2$, the simplest homoclinic bifurcation yields a higher-dimensional ($2p + 4$ -dimensional) reduced system, with supplementary pairs of simple imaginary eigenvalues of the linearized operator (the imaginary part of the spectrum consists of a pair of double eigenvalues and p pairs of simple ones). By analogy with results of Lombardi [30], it has been conjectured [28, 42] that the above mentioned solutions of the truncated normal form homoclinic to 0 do not *generically* persist when higher order terms are taken into account in the normal form. Persistence might be true if parameters $(T, \gamma, \text{coefficients in the Taylor expansion of } V)$ are chosen on a discrete collection of codimension- p submanifolds of the parameter space. For general parameter values, instead of orbits homoclinic to 0 one can expect the existence of reversible orbits homoclinic to exponentially small p -dimensional tori, originating from the p additional pairs of simple purely imaginary eigenvalues. These solutions should constitute the principal part of exact travelling breather solutions of (1) superposed on a small quasi-periodic oscillatory tail. However, in order to obtain exact

solutions one has to prove the persistence of the corresponding homoclinic orbits as higher order terms are taken into account in the normal form. This step is non-trivial and would require to generalize results of Lombardi [30] available for a single pair of simple imaginary eigenvalues (another promising approach is developed in the recent work [26]).

One might think that this nonpersistence picture contrasts with the case of the integrable Ablowitz-Ladik lattice [1], which supports an explicit family of exact travelling breather solutions in which the breather velocity can be varied continuously. However these solutions are not robust under various non-Hamiltonian reversible perturbations as shown in [6].

In this paper we numerically solve system (4) in the case $p = 2$, which constitutes the simplest situation for travelling breather solutions (the case $p = 1$ corresponding to travelling waves). This allows us to go beyond the analytical results obtained in [28], which were restricted to the small amplitude regime.

Our numerical observations confirm that system (1)-(2) (with $p = 2$) admits travelling breather solutions superposed on a small oscillatory tail. These solutions are either weakly or strongly localized depending on the value of T (γ being fixed). These results are obtained both for hard and soft on-site potentials. In addition we provide examples where the tail's amplitude can be made extremely small near particular values of the breather velocity, which makes the tail difficult to detect at the scale of central oscillations. Note that travelling breather solutions have been previously computed in the DNLS equation [17, 2] (in fact gauge symmetry reduces the problem to the computation of travelling waves), but the possible existence of a very small oscillatory tail has not been addressed.

An intuitive explanation for the existence of a tail is that travelling breathers transfer energy to resonant phonons. The energy transfer can be balanced by the superposition of a resonant phonon tail, which allows the breathers to propagate in an exact way. This remark might suggest more generally that a way to enhance breather mobility in nonlinear oscillator chains could be to excite resonant phonons with appropriate amplitudes.

Our numerical computations are performed as follows. We consider system (4) for $p = 2$ and rescale time by setting $t = \frac{\tau}{T}$. We introduce the variable $(u_1(t), u_2(t)) = (x_1(\tau), x_2(\tau + \frac{T}{2}))$, which is a solution of the symmetrized system

$$\frac{d^2}{dt^2} \begin{bmatrix} u_1 \\ u_2 \end{bmatrix} + T^2 \begin{bmatrix} V'(u_1) \\ V'(u_2) \end{bmatrix} = \gamma T^2 \begin{bmatrix} u_2(t - \frac{1}{2}) - 2u_1(t) + u_2(t + \frac{1}{2}) \\ u_1(t + \frac{1}{2}) - 2u_2(t) + u_1(t - \frac{1}{2}) \end{bmatrix} \quad (5)$$

and is related with the original variables by the relations

$$\begin{aligned} x_n(\tau) &= u_1(\frac{\tau}{T} - \frac{n-1}{2}) \text{ if } n \text{ is odd,} \\ x_n(\tau) &= u_2(\frac{\tau}{T} - \frac{n-1}{2}) \text{ if } n \text{ is even.} \end{aligned} \quad (6)$$

We solve system (5) by finite difference discretization and a Newton method (the Powell hybrid method [34]). An alternative would be to use spectral methods, as done in [16, 14, 38, 4] for the computation of travelling waves.

In addition, we derive a simpler problem in the case of even potentials V . In this case, system (5) admits symmetric solutions satisfying $u_1 = -u_2$, corresponding to solutions of (1) having the form

$$x_n(\tau) = (-1)^{n+1} u_1 \left(\frac{\tau}{T} - \frac{(n-1)}{2} \right). \quad (7)$$

This yields a new scalar advance-delay differential equation

$$\frac{d^2 u_1}{dt^2} + T^2 V'(u_1) = -\gamma T^2 (u_1(t + 1/2) + 2u_1(t) + u_1(t - 1/2)). \quad (8)$$

The convergence of the Newton method heavily relies on having a good initial guess. For this purpose we use the explicit principal parts of solutions provided by center manifold theory in the small amplitude regime [28], and continue them numerically by varying T .

An alternative numerical method would be to consider equation (1) and search for fixed points of the time- T map $F : (x_n(0), \dot{x}_n(0)) \mapsto (x_{n+p}(T), \dot{x}_{n+p}(T))$, which correspond to solutions satisfying (2). This method has been used in [5] for $p = 1$ (case of travelling waves). The first step of the method consists in computing a static breather, which is then perturbed in the direction of a pinning mode in order to obtain a (slowly moving) approximate travelling breather. This solution serves in turn as an initial guess for the Newton method, as one computes fixed points of F . One limitation of the method is that pinning modes do not always exist (this is the case e.g. for certain hard quartic on-site potentials), but the method yields very precise results at least for travelling waves [5].

The paper is organized as follows. Section 2 describes the numerical scheme and suitable initial guesses for the Newton method. Section 3 is devoted to the scalar case (8). System (5) is numerically solved in section 4.

2 Numerical method

2.1 Finite difference scheme

Equations (5) and (8) have the following general form

$$\frac{d^2 U}{dt^2} + W(U) = \sum_{j=-1}^1 A_j U(t + \frac{j}{2}), \quad (9)$$

where $U(t) \in \mathbb{R}^d$ ($d = 1, 2$) and A_{-1}, A_0, A_1 are $d \times d$ matrix. The nonlinear function $W : \mathbb{R}^d \rightarrow \mathbb{R}^d$ is smooth and satisfies $W(0) = 0$. We consider periodic boundary conditions $U(t + M) = U(t)$. For large M one can expect to find good approximations to spatially localized solutions which have “infinite period” (in practice we shall fix $M = 20$ most of the time).

We shall approximate (9) using a second order finite difference scheme. We choose the interval of discretization $I = [-\frac{M}{2}, \frac{M}{2}]$ and a discretization step $h = \frac{1}{2N}$ where $M, N \in \mathbb{N}^*$. We fix an integer period M so that time delays in (9) will be multiple of the step size, but this feature is not essential (see section 3.3).

We set $U_i = U(hi)$ with $hi \in I$ and $i = -MN + 1, \dots, MN$. The finite difference scheme writes

$$\frac{U_{i+1} - 2U_i + U_{i-1}}{h^2} + W(U_i) = \sum_{j=-1}^1 A_j U_{i+jN}, \quad (10)$$

for $i = -MN + 1, \dots, MN$. We impose the following periodic boundary conditions

$$U_{i+2MN} = U_i. \quad (11)$$

Equations (10)-(11) lead to a nonlinear system of $2MN$ equations with $2MN$ unknowns U_i . We use a Powell hybrid method [34] to solve this system (we impose a stopping criteria at precision of 10^{-12}).

Numerical solutions of (9) obtained by solving (10)-(11) are checked by an integration of system (1) with $(x_n(0), \dot{x}_n(0))$ as initial condition (x_n is deduced from equation (6) or (7), and one considers $2M$ lattice sites with periodic boundary conditions). The numerical integration is performed with a 4th order Runge-Kutta scheme. We impose that x_n is shifted by 2 sites after integration over $[0, T]$ with a relative error tolerance of order 10^{-5} . Figure 1 gives a typical profile of the evolution of the relative error as a function of step h (note that the error decays as h^2).

The crucial step is the choice of a good initial guess for the Powell method. This aspect is examined in next section.

2.2 Initial guess

The existence of small amplitude travelling breather solutions of (1) (having a small oscillatory tail) has been proved in [28] in the case of even potentials, using a center manifold technique. The method also provides leading order approximate expressions for these solutions (these approximate expressions are also available in the case of asymmetric potentials). This material is described below.

We consider the linearization of system (5) at $(u_1, u_2) = (0, 0)$ and search for solutions of the linearized problem in the form $(u_1, u_2) = e^{iqt}(\hat{u}_1, \hat{u}_2)^T$. This leads

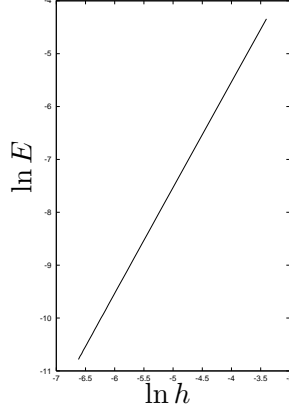


Figure 1: Relative error $E = \|\{x_n(T) - x_{n-2}(0)\}\| / \|\{x_n(T)\}\|$ ($\|\cdot\|$ denotes the Euclidean norm) as a function of step h (in logarithmic scales), for a travelling breather solution at $T = 7.7$, $\gamma \approx 0.9$, with the polynomial potential $V(x) = \frac{1}{2}x^2 - \frac{1}{4}x^4$.

to the following dispersion relation

$$(-q^2 + T^2(1 + 2\gamma))^2 - 4(\gamma T^2)^2 \cos^2(q/2) = 0. \quad (12)$$

Equation (12) provides the spectrum (consisting in eigenvalues $\pm iq$) of a certain linearized evolution operator obtained as system (5) is rewritten in the form of a reversible differential equation in a Banach space (see [28] for more details). The spectrum on the imaginary axis corresponds to solutions $q \in \mathbb{R}$ of (12) and is sketched in figure 2.

Double roots $q \in \mathbb{R}$ of (12) satisfy in addition

$$2q(-q^2 + T^2(1 + 2\gamma)) = (\gamma T^2)^2 \sin(q) \quad (13)$$

(solutions of (12)-(13) correspond to eigenvalues of the linearized evolution operator which are in general double, and at most triple [28]). We note that for $T^2(1 + 2\gamma) = (2k + 1)^2\pi^2$ ($k \in \mathbb{N}$), $q = (2k + 1)\pi$ is a double root of (12). This situation occurs on the curves denoted as Σ_4 in figure 2, and corresponds to the crossing of two simple roots of (12) as these curves are crossed in the parameter plane. The other double roots defined by system (12)-(13) are found as parameters lie on the curve $\Gamma : (T(q), \gamma(q))$ ($q \in \mathbb{R}^+$) defined by

$$T^2 = q^2 - 4q \tan(q/4), \quad (14)$$

$$\gamma = \frac{2q}{T^2 \sin(q/2)}, \quad (15)$$

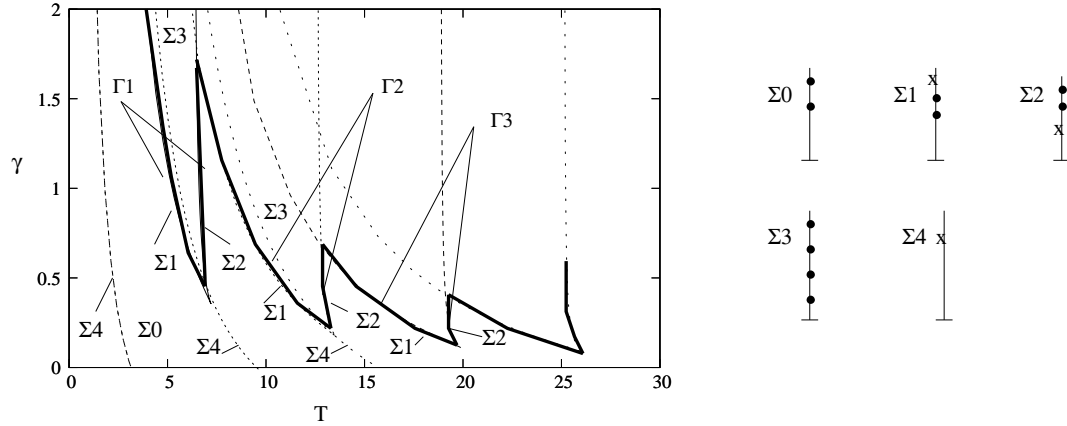


Figure 2: Sketch of the eigenvalues iq on the upper imaginary axis (right), in different regions of the parameter space (left). These eigenvalues correspond to real solutions of (12) (here $q > 0$).

if $q \in [4k\pi, (2k+1)2\pi]$ (for an integer $k \geq 1$), and

$$T^2 = q^2 + \frac{4q}{\tan(q/4)}, \quad (16)$$

$$\gamma = -\frac{2q}{T^2 \sin(q/2)}, \quad (17)$$

if $q \in [(2k-1)2\pi, 4k\pi]$ ($k \geq 1$). The range of q is determined by the condition $T^2 > 0$. One can observe that Γ lies in the parameter region $\gamma T^2 > 4$.

We denote by Γ_k the restriction of Γ to the interval $q \in [2k\pi, 2(k+1)\pi]$ (these curves form “tongues” as shown in figure 2). Our numerical computations will start near Γ_1 where bifurcation of small amplitude travelling breathers take place. Travelling breathers bifurcate more generally near Γ_{2k+1} [28], and bifurcating solitary waves are found near Γ_{2k} [25].

Double roots on Γ correspond to the appearance (or vanishing) of a pair of real roots of (12) as the curve Γ is crossed. The envelope Δ of Γ is the bold line depicted in figure 2. Below it (and outside Σ_4), real solutions of (12) consist in two pairs of simple roots $\pm q_1, \pm q_2$. An additional pair of real (double) roots $\pm q_0$ appears as one reaches Δ from below (they correspond to pairs of hyperbolic eigenvalues of the linearized evolution operator colliding on the imaginary axis). In the sequel, we shall exclude points of Δ which are close to points where $sq_0 + rq_1 + r'q_2 = 0$ for $s, r, r' \in \mathbb{Z}$ and $0 < |s| + |r| + |r'| \leq 4$ (such values correspond to strong resonances), and denote this new set as Δ_0 .

Now we fix $(T_0, \gamma_0) \in \Gamma_m \cap \Delta_0$. For $(\gamma, T) \approx (\gamma_0, T_0)$, it has been proved in [28] that small amplitude solutions of (5) have the form

$$\begin{pmatrix} u_1(t) \\ u_2(t) \end{pmatrix} = A(t) \begin{pmatrix} (-1)^m \\ 1 \end{pmatrix} + C(t) \begin{pmatrix} -1 \\ 1 \end{pmatrix} + D(t) \begin{pmatrix} 1 \\ 1 \end{pmatrix} + \text{c.c.} + \Psi(u_c(t), \gamma, T), \quad (18)$$

where $u_c = (A, B, C, D, \bar{A}, \bar{B}, \bar{C}, \bar{D})^T \in \mathbb{C}^8$ and $\Psi : \mathbb{C}^8 \times \mathbb{R}^2 \rightarrow \mathbb{R}^2$ is a smooth function, with $\Psi(u_c, \gamma, T) = O(\|u_c\|^2 + \|u_c\|(|\gamma - \gamma_0| + |T - T_0|))$ as $(u_c, \gamma, T) \rightarrow (0, \gamma_0, T_0)$ (i.e. Ψ contain higher order terms). The complex coordinates (A, B, C, D) satisfy a reversible differential equation

$$\begin{aligned} \frac{dA}{dt} &= iq_0 A + B + iA\mathcal{P}(v_1, v_2, v_3, v_4) + O((|A| + |B| + |C| + |D|)^4), \\ \frac{dB}{dt} &= iq_0 B + iB\mathcal{P}(v_1, v_2, v_3, v_4) + A\mathcal{S}(v_1, v_2, v_3, v_4) \\ &\quad + O((|A| + |B| + |C| + |D|)^4), \\ \frac{dC}{dt} &= iq_1 C + iC\mathcal{Q}(v_1, v_2, v_3, v_4) + O((|A| + |B| + |C| + |D|)^4), \\ \frac{dD}{dt} &= iq_2 D + iD\mathcal{T}(v_1, v_2, v_3, v_4) + O((|A| + |B| + |C| + |D|)^4), \end{aligned} \quad (19)$$

where

$$v_1 = A\bar{A}, v_2 = C\bar{C}, v_3 = D\bar{D}, v_4 = i(A\bar{B} - \bar{A}B)$$

and $\mathcal{P}, \mathcal{S}, \mathcal{Q}, \mathcal{T}$ are affine functions with smoothly parameters dependent real coefficients, for (T, γ) in the neighborhood of Δ_0 . We have

$$\begin{aligned} \mathcal{P}(v_1, v_2, v_3, v_4) &= p_1(\gamma, T) + p_2 v_1 + p_3 v_2 + p_4 v_3 + p_5 v_4, \\ \mathcal{S}(v_1, v_2, v_3, v_4) &= s_1(\gamma, T) + s_2 v_1 + s_3 v_2 + s_4 v_3 + s_5 v_4, \\ \mathcal{Q}(v_1, v_2, v_3, v_4) &= \tilde{q}_1(\gamma, T) + \tilde{q}_2 v_1 + \tilde{q}_3 v_2 + \tilde{q}_4 v_3 + \tilde{q}_5 v_4, \\ \mathcal{T}(v_1, v_2, v_3, v_4) &= t_1(\gamma, T) + t_2 v_1 + t_3 v_2 + t_4 v_3 + t_5 v_4 \end{aligned} \quad (20)$$

where $p_1, s_1, \tilde{q}_1, t_1$ vanish on Δ_0 . The method for computing the coefficients of (20) is given e.g. in [28], section 5.2 (see [24] for a description of the method in a general setting). Defining the coefficients in the expansion of V as

$$V(x) = \frac{1}{2}x^2 + \frac{\alpha}{3}x^3 + \frac{\beta}{4}x^4 + O(|x|^5), \quad x \rightarrow 0, \quad (21)$$

one has in particular for $(T, \gamma) = (T_0, \gamma_0) \in \Delta_0$

$$(2 - \frac{q_0}{\tan(q_0/2)})s_2 = T_0^2(-6\beta + 8\alpha^2 - \frac{4\alpha^2 T_0^2}{2\gamma_0 T_0^2 \cos(q_0) - T_0^2(1 + 2\gamma_0) + 4q_0^2}). \quad (22)$$

Moreover, as $(T, \gamma) \rightarrow (T_0, \gamma_0) \in \Delta_0$ one has

$$s_1 = s_{11}(\gamma - \gamma_0) + s_{12}(T - T_0) + \text{h.o.t.},$$

with

$$s_{11} = -4T_0^2 \frac{\epsilon - \cos(q_0/2)}{2\epsilon - \frac{\gamma_0 T_0^2}{2} \cos(q_0/2)}, \quad s_{12} = 4T_0 \frac{-(1 + 2\gamma_0)\epsilon + 2\gamma_0 \cos(q_0/2)}{2\epsilon - \frac{\gamma_0 T_0^2}{2} \cos(q_0/2)}. \quad (23)$$

We set $\epsilon = -1$ in (23) if $q_0 \in [(2k-1)2\pi, 4k\pi]$, $k \geq 1$ (i.e. $(T_0, \gamma_0) \in \Gamma_{2k-1}$) and $\epsilon = 1$ if $q_0 \in [4k\pi, (2k+1)2\pi]$ ($(T_0, \gamma_0) \in \Gamma_{2k}$).

Equation (18) expresses the fact that small solutions of (5) lie on a 8-dimensional center manifold $\mathcal{M}_{\gamma, T}$, the dimension of which is equal to the number of marginal modes of equation (5) linearized at $(u_1, u_2) = 0$ for $(\gamma, T) = (\gamma_0, T_0)$. One can parametrize the center manifold in such a way that the reduced system (i.e. the 8-dimensional differential equation satisfied by the coordinates u_c of solutions on $\mathcal{M}_{\gamma, T}$) is as simple as possible (this form is called “normal form”). The normal form of order 3 of the reduced system is given in (19). The truncated normal form (obtained by neglecting terms of orders 4 and higher in (19)) is integrable [27], [28].

For $(T, \gamma) \approx (T_0, \gamma_0) \in \Gamma_m \cap \Delta_0$ and if (T, γ) lies below Δ (this corresponds to having $s_1 > 0$ in (20)), the linearized operator at the right side of (19) admits two pairs of symmetric hyperbolic eigenvalues close to $\pm iq_0$, and two pairs of purely imaginary eigenvalues close to $\pm iq_1, \pm iq_2$. If $s_2(\gamma_0, T_0) < 0$, the *truncated* normal form admits reversible homoclinic solutions to 0 which bifurcate from the trivial state as $(T, \gamma) \rightarrow (T_0, \gamma_0)$. They correspond near Γ_{2k+1} to *approximate* travelling breather solutions of (1), given by system (5) and having the form

$$\begin{pmatrix} u_1(t) \\ u_2(t) \end{pmatrix} \approx A(t) \begin{pmatrix} -1 \\ 1 \end{pmatrix} + \text{c.c.}$$

(this expression comes from the principal parts of (18),(19)), where

$$A(t) = r_0(t) e^{i(q_0 t + \psi(t))}, \quad (24)$$

and

$$r_0(t) = \left(\frac{2s_1}{-s_2}\right)^{1/2} (\cosh(ts_1^{1/2}))^{-1}, \quad \psi(t) = p_1 t + 2\frac{p_2}{s_2} s_1^{1/2} \tanh(ts_1^{1/2}). \quad (25)$$

The ansatz (24) provides a good initial guess for computing small amplitude travelling breather solutions with the Powell method. The solutions initially computed are then followed by continuation as a function of T towards higher amplitudes.

The normal form coefficients p_1, p_2 in (25) can be computed as explained in [24]. However, the term $\psi(t)$ in (24) is negligible as $(T, \gamma) \approx (T_0, \gamma_0)$ since $p_1, s_1 \approx 0$ and $t \in [-\frac{M}{2}, \frac{M}{2}]$. Consequently one can fix $\psi = 0$ in (24) to initiate the Powell method.

In addition, it is not necessary to take oscillatory modes $C(t), D(t)$ into account in the initial ansatz (24) because those are conjectured to be exponentially small with respect to $|\gamma - \gamma_0| + |T - T_0|$ as $(\gamma, T) \rightarrow (\gamma_0, T_0)$, for some exact solutions of (5) (this has been proved for even potentials [28]). Note in addition that a tail appears naturally as one iterates the Powell method.

In the following section, we present numerical computations in a particular symmetric case (for even potentials V) in which travelling breather solutions are given by a scalar advance-delay differential equation.

3 Case of even potentials V

We consider the case when the potential V in (1) is even. In this case, there exist solutions of (1) satisfying

$$x_{n+1}(\tau) = -x_n(\tau - \frac{T}{2}), \quad (26)$$

given by the scalar advance-delay differential equation (8). Section 3.1 reviews analytical results [28] concerning small amplitude travelling breather solutions of the form (26). These solutions are numerically computed in section 3.2 and continued into the large amplitude regime. In section 3.3 we numerically identify these solutions as modulations of certain time-periodic oscillations (time-periodic pulsating travelling waves).

3.1 Exact small amplitude travelling breathers

In this section we sum up analytical results obtained in [28], which follow from the center manifold reduction theorem and the analysis of the reduced equation (19).

The homoclinic orbits of the truncated normal form described in section 2.2 bifurcate near parts of the “tongues” Γ_m where $s_2 < 0$. For even potentials ($\alpha = 0$ in (21)), homoclinic bifurcations occur near left branches of Γ_m if V is hard ($\beta > 0$ in (21)), and near right branches if V is soft ($\beta < 0$). The situation is depicted in figure 3 (see [28] for more details).

Now assume $s_2(\gamma_0, T_0) < 0$ defined by equation (22) for a fixed $(T_0, \gamma_0) \in \Delta_0 \cap \Gamma_{2k+1}$ and consider $(\gamma, T) \approx (\gamma_0, T_0)$, (T, γ) lying below Δ in the parameter plane. The full reduced equation (19) admits an invariant subspace defined by

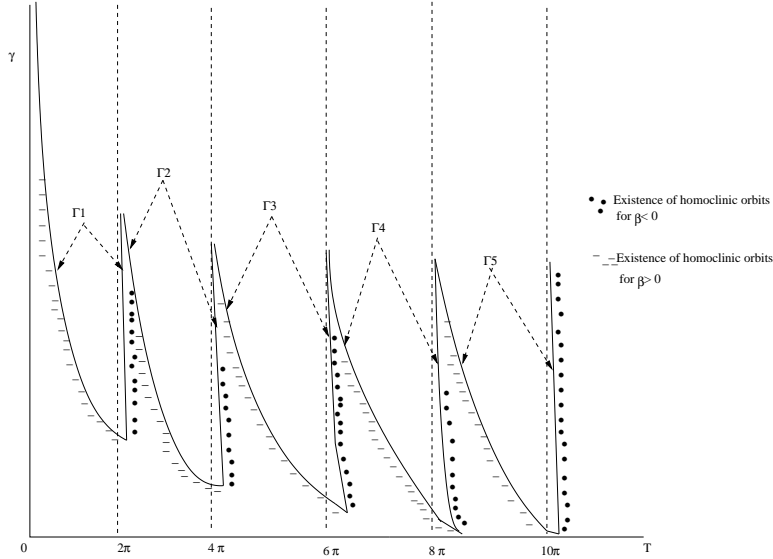


Figure 3: Regions in the parameter space where small amplitude homoclinic orbits to 0 bifurcate for the truncated normal form (case of an even potential).

$D = 0$ due to the evenness of V (see [28]). Considering (19) on this invariant subspace is equivalent to searching for solutions of (1)-(2) satisfying (26) ($m = 2k + 1$ and $u_2 = -u_1$ in (18)).

If (T_0, γ_0) lies outside some subset of $\Delta_0 \cap \Gamma_{2k+1}$ having zero Lebesgue measure (corresponding to resonant cases), the full reduced equation (19) admits small amplitude reversible solutions (with $D = 0$) homoclinic to periodic orbits. These solutions correspond to *exact* travelling breather solutions of system (1) superposed at infinity on an oscillatory (periodic) tail. Their principal part is given by

$$x_n(\tau) = (-1)^n [A + C] \left(\frac{\tau}{T} - \frac{n-1}{2} \right) + \text{c.c.} + \text{h.o.t.}, \quad (27)$$

where (A, C) is a solution of (19) homoclinic to a periodic orbit (see [28] for an approximation of (A, C) at leading order). For a fixed value of (γ, T) (and up to a time shift), these solutions occur in a one-parameter family parametrized by the amplitude of oscillations at infinity. The lower bound of these amplitudes is $O(e^{-c/\mu^{1/2}})$, where $\mu = |T - T_0| + |\gamma - \gamma_0|$, $c > 0$.

The lower bound of the amplitudes should be *generically* nonzero, but may vanish on a discrete collection of curves in the parameter plane (T, γ) . As a consequence, in a given system (1) (with fixed coupling constant γ and symmetric on-site potential V), exact travelling breather solutions decaying to 0 at infinity (and satisfying (2) for $p = 2$) may exist in the small amplitude regime, for isolated

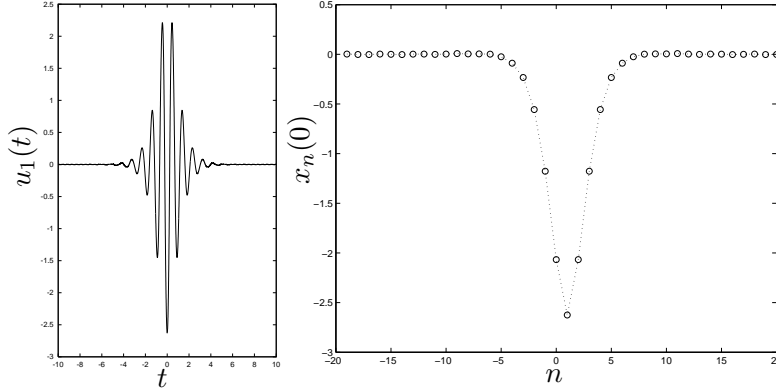


Figure 4: Large amplitude solution in the case of the trigonometric potential $V(x) = 1 - \cos(x)$ with $T = 8.1$, $\gamma = \gamma_0 \approx 0.9$, $T_0 \approx 6.63$ ($(T_0, \gamma_0) \in \Gamma_1$). The left figure shows the displacements of mass $n = 1$ as a function of t (note that t is a rescaled time). The right one shows displacements for all lattice sites at time $\tau = 0$.

values of the breather velocity $2/T$.

In the following section, we fix $(T_0, \gamma_0) \in \Gamma_1$ and consider $\mu = |T - T_0|$ as a small parameter, $\gamma = \gamma_0$ being fixed. We numerically solve equation (8) and follow the above mentioned travelling breather solutions into the large amplitude regime.

3.2 Numerical computation of travelling breathers

Let us consider the trigonometric potential $V(x) = 1 - \cos(x)$ ($\beta = -\frac{1}{6}$ in (21)) and fix $\gamma \approx 0.9$, $T = 8.1$. These parameter values lie near the existence domain of small amplitude travelling breather solutions (see section 3.1). However, parameters are chosen sufficiently far from the curve Γ_1 on which travelling breathers bifurcate (the point $(T_0, \gamma_0) \approx (6.63, 0.9)$ lies on Γ_1), and correspond thereby to highly localized solutions. Figure 4 shows a solution $u_1(t)$ of (8) (left), and the displacements of lattice sites at time $\tau = 0$ deduced from equation (7) (right).

This result shows that the Klein-Gordon lattice with a trigonometric potential supports highly localized travelling breather solutions. Although the solution in figure 4 seems perfectly localized, it admits in fact a small oscillatory tail not visible at the figure scale (this phenomenon is known for small amplitude solutions, see section 1). The tail is clearly visible after magnification (figure 5).

In the sequel we study in more detail the properties of these solutions as T is varied, and depending whether one considers a hard or soft on-site potential. For this purpose we shall fix $V(x) = \frac{1}{2}x^2 + \frac{\beta}{4}x^4$. Figure 6 presents numerically

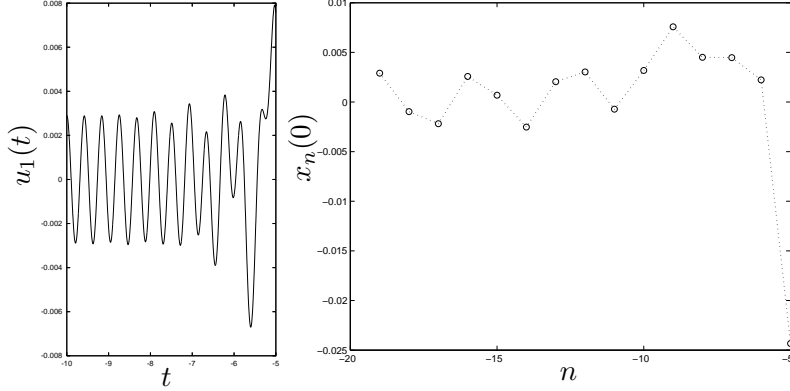


Figure 5: Magnification of the solution tail in figure 4 (case of a trigonometric potential V , $T = 8.1$, $\gamma \approx 0.9$).

computed solutions of (8) for different values of the propagation time T . Left column corresponds to the hard potential $V(x) = \frac{1}{2}x^2 + \frac{1}{24}x^4$ ($\beta = 1/6$), the right one to the soft potential $V(x) = \frac{1}{2}x^2 - \frac{1}{4}x^4$ ($\beta = -1$). We start close to parameter values $(T_0, \gamma_0) \in \Gamma_1 \cap \Delta_0$ and fix $\gamma = \gamma_0$.

One can check that as $\mu = |T - T_0|$ increases, the central peak of the solution gets more localized and increases in amplitude. In addition, a periodic tail becomes more visible as μ increases. One can observe a frequency difference between the central part of solutions and their tail, as it is the case in the small amplitude regime (in equation (27), the central part $A(t)$ and the tail $C(t)$ oscillate respectively with frequencies close to the linear frequencies q_0 and q_1). In particular the tail has a lower frequency in the case of hard potentials, and a larger one for soft potentials. In figure 7 we plot the Fourier spectrum of $u_1(t)$ for two profiles of figure 6 (hard and soft potential case). The tail frequency and the central part internal frequency are found relatively close to the linear frequencies q_1 and q_0 .

In figure 8 we compare the tail of a localized solution of figure 6 with a numerically computed periodic solution (a nonlinear normal mode) originating from the eigenvalues $\pm iq_1$ (the existence of such solutions is guaranteed by the Lyapunov-Devaney theorem). The tail of the localized solution is very close to the periodic solution, which confirms that the large amplitude localized solution can be seen as “homoclinic to periodic”, as in the small amplitude regime.

In figure 9 we plot as a function of n a travelling breather solution of (1) corresponding (via equation (7)) to a profile of figure 6. In the case of a hard potential one observes that most neighboring oscillators are out of phase near the breather center. The case of a soft potential is considered in figure 10, which shows that neighboring oscillators are in phase near the center.

Now let us examine the amplitude of travelling breathers versus parameter μ

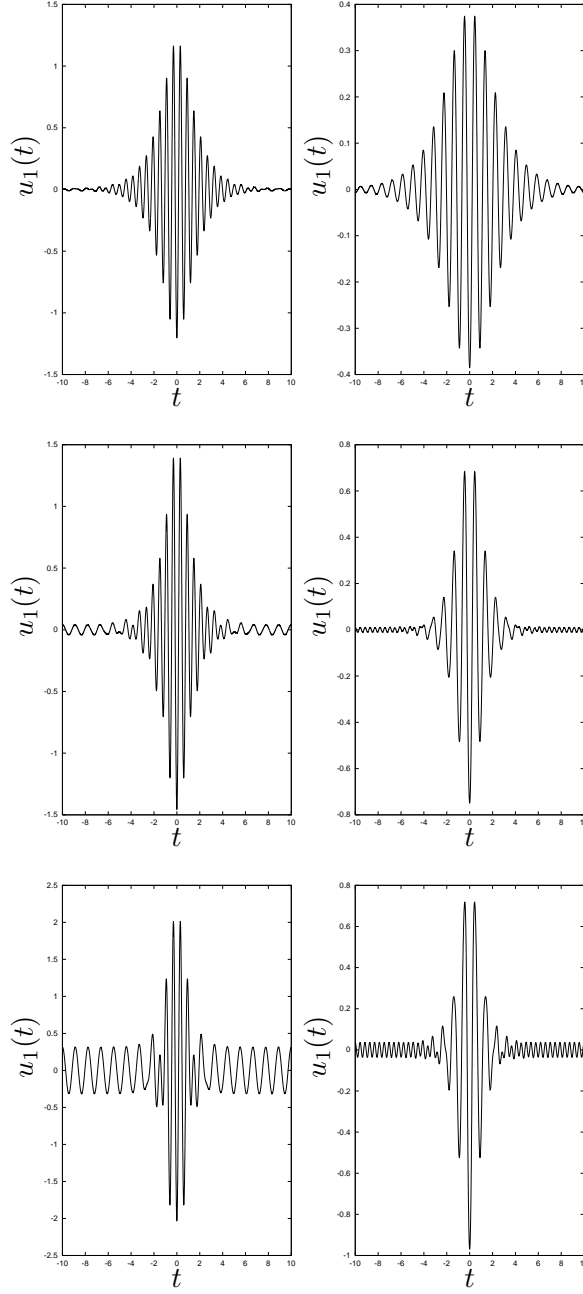


Figure 6: Localized numerical solutions of (8) for various propagation times T and polynomial potentials $V(x) = \frac{1}{2}x^2 + \frac{\beta}{4}x^4$. The left figures correspond to a hard potential ($\beta = 1/6$, $\gamma = \gamma_0 \approx 0.83$, $T_0 \approx 5.59$ and $T = 5.53$, $T = 5.5$, $T = 5.35$ from top to bottom) and the right ones to a soft potential ($\beta = -1$, $\gamma = \gamma_0 \approx 0.9$, $T_0 \approx 6.63$ and $T = 6.8$, $T = 7.4$, $T = 8.1$ from top to bottom). The value of $\mu = |T - T_0|$ increases from top to bottom.

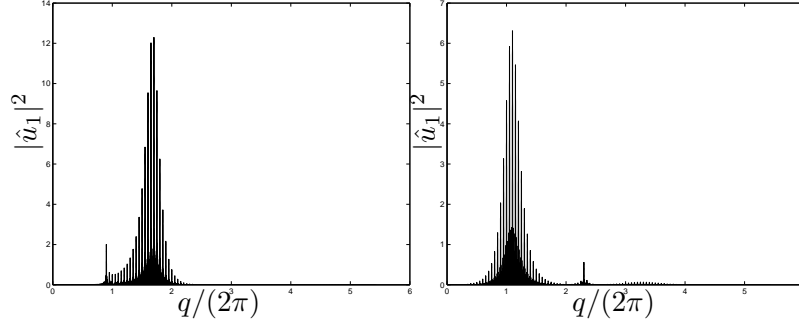


Figure 7: Fourier spectra of $u_1(t)$ (profiles of figure 6 are extended with periodic boundary conditions). The right figure corresponds to a solution at $T = 7.4$, $\gamma = \gamma_0 \approx 0.9$, $T_0 \approx 6.63$ for $V(x) = \frac{1}{2}x^2 - \frac{1}{4}x^4$ (see figure 6, right). The left one corresponds to a solution at $T = 5.5$, $\gamma = \gamma_0 \approx 0.83$, $T_0 \approx 5.59$ for $V(x) = \frac{1}{2}x^2 + \frac{1}{24}x^4$ (see figure 6, left). The peaks are relatively close to $q_0/2\pi \approx 1.11$, $q_1/2\pi \approx 2.30$ in the soft potential case and $q_0/2\pi \approx 1.7$, $q_1/2\pi \approx 0.9$ in the hard case.

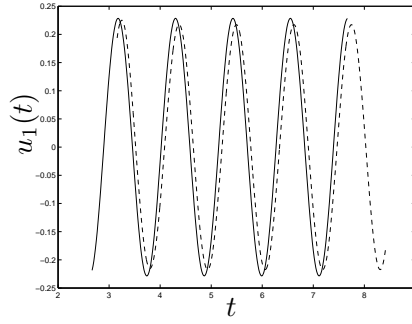


Figure 8: Comparison of a nonlinear normal mode issued from the eigenvalues $\pm i q_1$ (continuous line) with the tail of a localized solution of figure 6 (dotted line), for $T = 5.35$ and $V(x) = \frac{1}{2}x^2 + \frac{1}{24}x^4$. We have $\gamma = \gamma_0 \approx 0.83$, $T_0 \approx 5.59$ and $(T_0, \gamma_0) \in \Gamma_1$.

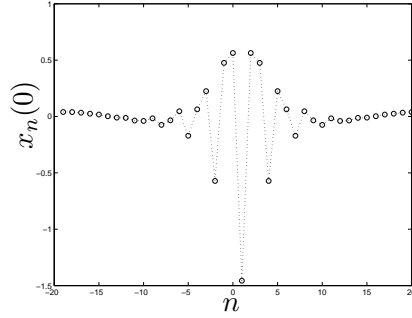


Figure 9: Numerical solution of (1)-(2) for $T = 5.5$ and $p = 2$. We consider $V(x) = \frac{1}{2}x^2 + \frac{1}{24}x^4$, $\gamma = \gamma_0 \approx 0.83$, $T_0 \approx 5.59$ $((T_0, \gamma_0) \in \Gamma_1)$. The solution is plotted as a function of n , for $\tau = 0$, and corresponds via equation (7) to a solution $u_1(t)$ in figure 6 (left column, middle).

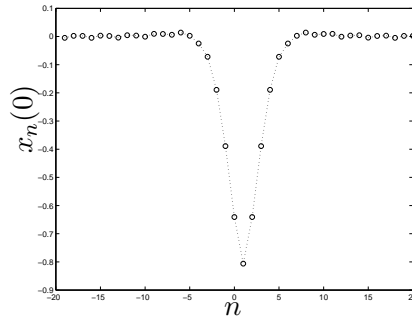


Figure 10: Numerical solution of (1)-(2) for $T = 7.4$ and $p = 2$. We consider $V(x) = \frac{1}{2}x^2 - \frac{1}{4}x^4$, $\gamma = \gamma_0 \approx 0.9$, $T_0 \approx 6.63$ $((T_0, \gamma_0) \in \Gamma_1)$. The solution is plotted as a function of n , for $\tau = 0$, and corresponds via equation (7) to a solution $u_1(t)$ in figure 6 (right column, middle).

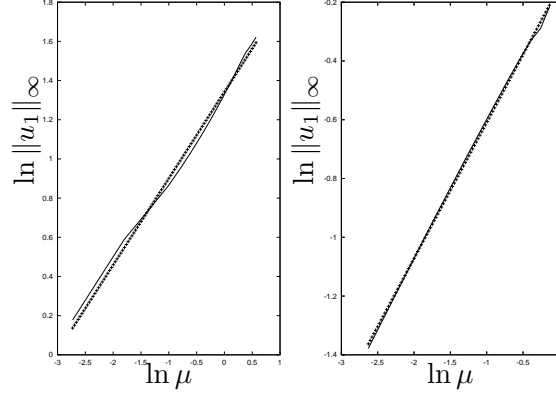


Figure 11: Maximal amplitude $\|u_1\|_\infty$ of a numerical solution of (8) (continuous line) as a function of μ in logarithmic scales. The dotted line represents a linear regression. One has $V(x) = \frac{x^2}{2} + \frac{x^4}{24}$, $\gamma = \gamma_0 \approx 0.83$, $T_0 \approx 5.59$ for the left figure and $V(x) = \frac{x^2}{2} - \frac{x^4}{4}$, $\gamma = \gamma_0 \approx 0.9$, $T_0 \approx 6.63$ for the right one. In both cases one has $\mu = |T - T_0|$ and $(T_0, \gamma_0) \in \Gamma_1$.

in the large amplitude regime. In figure 11 we plot the amplitude of solutions for polynomial potentials $V(x) = \frac{x^2}{2} + \frac{\beta}{4}x^4$. One finds that the amplitude behaves approximately as μ^δ for relatively large values of μ (corresponding to highly localized solutions), with $\delta \approx 0.44$ for the hard potential (with $\beta = 1/6$) and $\delta \approx 0.46$ for the soft one (with $\beta = -1$). In this latter case the amplitude graph becomes less regular as one enters the next “tongue” Γ_2 (figure 2), which might indicate bifurcations occurring near the numerically computed solutions (this part is not visible in figure 11).

A $\mu^{1/2}$ dependency of the amplitude (at leading order) is expected in the small amplitude regime $\mu \approx 0$ [28]. Surprisingly a rather similar behaviour is observed in the large amplitude regime.

We have found in addition multibump solutions. Figure 12 shows e.g. a 2–bumps solution of equation (8) (note the reverse symmetry between the two bumps).

3.3 Modulated periodic solutions

As previously we consider $(T_0, \gamma_0) \in \Gamma_1 \cap \Delta_0$ and choose $\mu = |T - T_0|$ as a small parameter, $\gamma = \gamma_0$ being fixed. If one neglects higher order terms in the normal form (19), the reversible bifurcation near Γ_{2k+1} creates (in addition to homoclinic solutions) a three-parameter family of periodic solutions with $C = D = 0$ and

$$A_{\mu,\lambda,\theta}(t) = r e^{i(\Omega t + \theta)}, \quad B_{\mu,\lambda,\theta}(t) = i\lambda r e^{i(\Omega t + \theta)}, \quad (28)$$

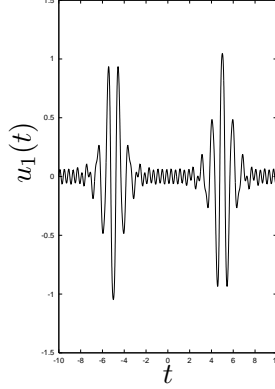


Figure 12: 2-bumps solution of equation (8). We consider $V(x) = \frac{1}{2}x^2 - \frac{1}{4}x^4$, $T_0 \approx 6.63$, $\gamma = \gamma_0 \approx 0.9$ ($(T_0, \gamma_0) \in \Gamma_1$) and $T = 9$.

provided one approaches Δ from below in figure 2 ($s_1 > 0$), $s_2 < 0$ and expression (28) is considered for $\lambda \approx 0$ (λ is a real parameter). The frequency Ω and modulus r depend on (μ, λ) as follows

$$\Omega - q_0 = \lambda + p_1 - (p_2 + 2\lambda p_5) \frac{\lambda^2 + s_1}{s_2 + 2\lambda s_5}, \quad (29)$$

$$r^2 = -\frac{\lambda^2 + s_1}{s_2 + 2\lambda s_5}. \quad (30)$$

Note that coefficients p_i, s_i depend on μ and the first integral v_4 of the truncated normal form takes the value $v_4 = i(A_{\mu, \lambda, \theta} \bar{B}_{\mu, \lambda, \theta} - \bar{A}_{\mu, \lambda, \theta} B_{\mu, \lambda, \theta}) = 2r^2\lambda$. The periodic solutions (28) are $O(\sqrt{\mu} + |\lambda|)$ as $(\mu, \lambda) \rightarrow 0$ (s_1 vanishes on Δ) and their frequency is close to q_0 (the colliding pair of double eigenvalues is $\pm iq_0$) since p_1 vanishes on Δ .

These solutions should correspond to solutions of (1) having the form

$$x_n(\tau) \approx 2(-1)^n r \cos \left[\Omega \left(\frac{\tau}{T} - \frac{n-1}{2} \right) + \theta \right] \quad (31)$$

at leading order, and consisting in time-periodic pulsating travelling waves. One has equivalently

$$\begin{pmatrix} u_1(t) \\ u_2(t) \end{pmatrix} \approx 2r \cos [\Omega t + \theta] \begin{pmatrix} -1 \\ 1 \end{pmatrix}. \quad (32)$$

To obtain exact solutions of (1) instead of leading order approximations, one should prove the persistence of the periodic solutions (28) as higher order terms are taken into account in the normal form (19). We shall not treat this question in the present paper and leave it for future works.

For computing the corresponding solutions of (9) with the same approach as in section 3.2, one has to consider the period M of solutions as a real parameter. The ansatz (32) is used with $\Omega = k\frac{2\pi}{M}$ (for an integer $k \geq 1$) to initiate the Powell method. Equations (29) and (30) determine $\lambda, r \approx 0$ locally as functions of the two parameters $\mu \approx 0$ and $M \approx k\frac{2\pi}{q_0}$ (hence $\Omega \approx q_0$). If we fix in addition $M - k\frac{2\pi}{q_0} = O(|\mu|)$, then equation (29) yields $\lambda = O(|\mu|)$ and we obtain $r^2 = -s_1/s_2 + O(\mu^2)$ using equation (30). Consequently we fix $r^2 = -s_1/s_2$ in the ansatz (32) to initiate the Powell method near the “tongue” Γ_1 .

To adapt the numerical scheme (10)-(11) to non-integer values of M , it suffices to rescale equation (8) into

$$\frac{d^2 y_1}{dx^2} + M^2 T^2 V'(y_1) = -M^2 \gamma T^2 (y_1(x + \frac{1}{2M}) + 2y_1(x) + y_1(x - \frac{1}{2M})), \quad (33)$$

where $y_1(x) = u_1(t)$, $x = \frac{t}{M}$ and (33) is subject to periodic boundary conditions $y_1(x+1) = y_1(x)$. One discretizes (33) with a scheme similar to (10)-(11), except advance and delay terms are now obtained by linear interpolation.

We have numerically observed that localized solutions bifurcate from the above family of periodic solutions as M is fixed and T is varied (figure 13). This property could be used to compute localized solutions by continuation from periodic solutions. This method has been previously employed in [17] for computing travelling breathers in the DNLS system. In this case the problem reduces to the computation of solitary waves, which bifurcate from families of (explicitly known) periodic travelling waves. This approach seems less efficient in our case since periodic solutions are not explicitly known and have to be computed numerically.

In the next section, we present numerical computations in the case of a non-even potential, corresponding to system (5).

4 Case of non even potentials V

4.1 Approximate solutions

The homoclinic orbits of the truncated normal form described in section 2.2 bifurcate near parts of the “tongues” Γ_m where $s_2 < 0$ (see equation (22)). In the case on non even potentials, these regions vary with the parameter

$$\kappa = \beta/\alpha^2, \quad (34)$$

depending on the quartic and squared cubic coefficients in the potential V (see (21)). The situation is depicted in figure 14 for the curve Γ_1 (see [28] for the detailed study of the sign of s_2).

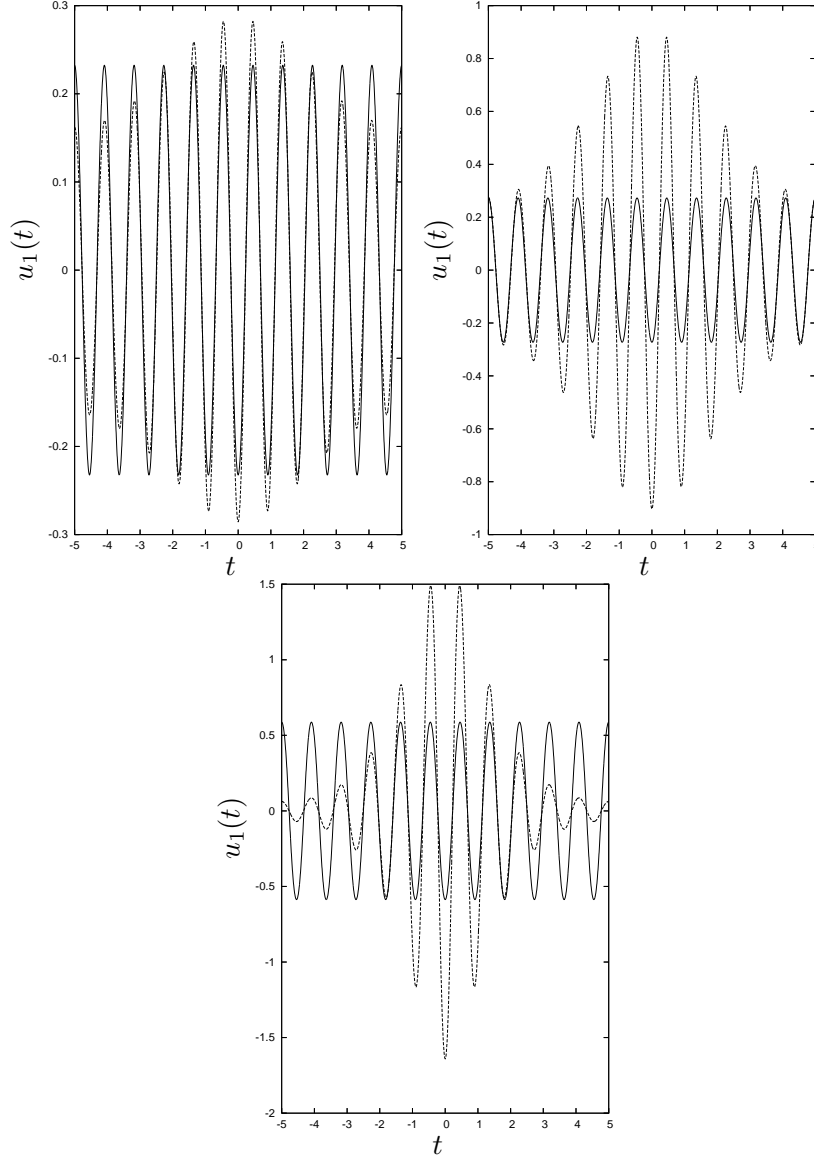


Figure 13: Comparison of a periodic solution (continuous line) with a weakly localized one (dotted line) for the soft polynomial potential $V(x) = \frac{1}{2}x^2 - \frac{1}{4}x^4$ and different values of T : $T = 6.75$ (top), $T = 6.8$ (middle), $T = 7.2$ (bottom). We have $\gamma = \gamma_0 \approx 0.9$ and $T_0 \approx 6.63$, $(T_0, \gamma_0) \in \Gamma_1$.

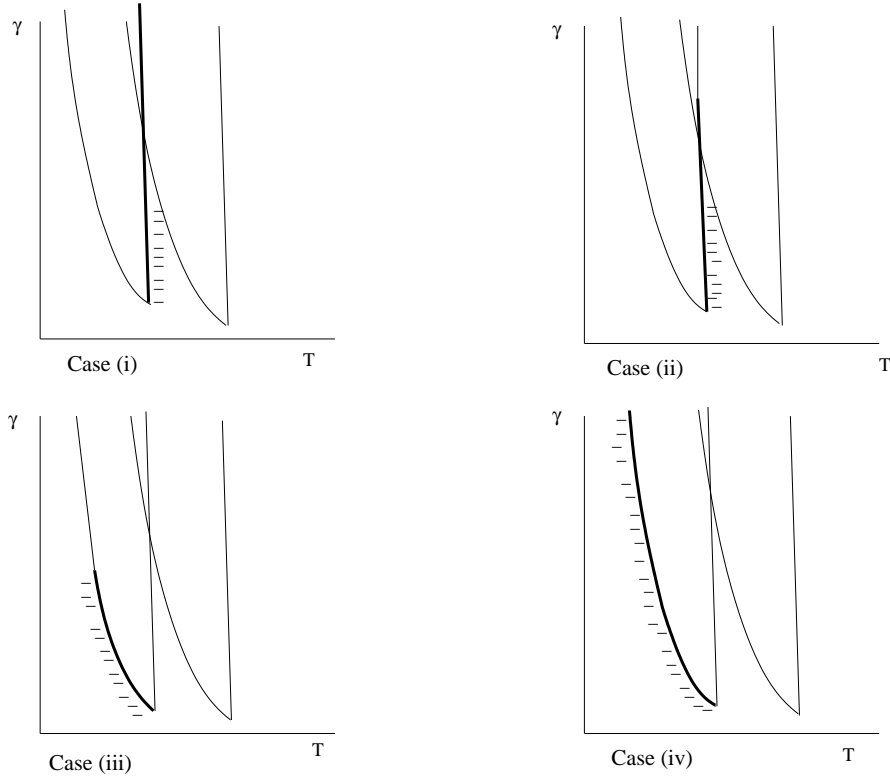


Figure 14: Part of Γ_1 where $s_2 < 0$ (bold line). The dashed area is a small neighborhood of this curve lying below Δ . It corresponds to regions where small amplitude homoclinic orbits to 0 bifurcate for the normal form (19) without higher order terms. The parameter κ defined by (34) varies as follows : (i) $\kappa < 10/9$, (ii) $10/9 < \kappa < \kappa_c$ with $\kappa_c \approx 1.15$, (iii) $\kappa_c < \kappa < 4/3$, (iv) $\kappa > 4/3$.

Now let us assume $s_2(\gamma_0, T_0) < 0$ for a fixed $(T_0, \gamma_0) \in \Delta_0 \cap \Gamma_{2k+1}$ and consider $(\gamma, T) \approx (\gamma_0, T_0)$, (T, γ) lying below Δ in the parameter plane. This is the case e.g. in the dashed area near Γ_1 depicted in figure 14.

Since V is non even, $D = 0$ is not in general an invariant subspace of the full normal form (19) and the oscillatory mode $D(t)$ cannot be eliminated as in section 3.1. In fact, one expects (this is still a conjecture) that bifurcating localized solutions have in general nonvanishing (up to an exponentially small size) oscillatory tails $D(t)$, $C(t)$ oscillating at (fast) frequencies close to q_2 , q_1 . These oscillations are combined with fast oscillations at a frequency close to q_0 (oscillatory part of $A(t)$) and the slow hyperbolic dynamics of the envelope of $A(t)$ (time scales are of order $1/\sqrt{\mu}$, $\mu = |T - T_0| + |\gamma - \gamma_0|$).

The normal form (19) *truncated at order 4* admits small amplitude solutions homoclinic to 2-tori (originating from the pairs of eigenvalues $\pm iq_1, \pm iq_2$). These approximate solutions of (19) have an explicit form (see [28], section 5.3). It has been conjectured in [28] that they should correspond to the principal part of travelling breather solutions of system (1), superposed at infinity on an oscillatory (quasiperiodic) tail, and given at leading order by the expression

$$x_n(\tau) \approx [(-1)^n A + (-1)^n C + D] \left(\frac{\tau}{T} - \frac{n-1}{2} \right) + \text{c.c.} \quad (35)$$

$((A, B, C, D)$ denotes one of the above mentioned approximate solutions of (19) homoclinic to a small quasiperiodic orbit). The persistence of these homoclinic solutions for the full normal form is still an open mathematical problem, which would require to generalize results of Lombardi [30] available when one of the oscillatory modes $C(t)$ or $D(t)$ is absent.

4.2 Numerical computation of travelling breathers

In this section we consider the Morse potential $V(x) = \frac{1}{2}(1 - e^{-x})^2$ and perform the same type of computations as in section 3.2, except we now work with system (5) instead of the scalar equation (8). We consider a point $(T_0, \gamma_0) \approx (6.63, 0.9)$ on Γ_1 , fix $\gamma = \gamma_0$ and let $\mu = T - T_0$ vary.

To initiate the Powell method we use the approximate travelling breather solutions described in section 2.2. For this purpose one has to choose (T, γ) near parts of Γ_1 where $s_2 < 0$, as described in section 4.1, figure 14 (dashed area). The Morse potential has the expansion (21) with $\alpha = -3/2$, $\beta = 7/6$, and $\kappa = 14/27$.

Figure 15 presents numerically computed solutions of (5) for different values of T . We only plot $u_1(t)$ because $u_2(t)$ behaves similarly. As $\mu = T - T_0$ increases, the central hump of the solution gets more localized and increases in amplitude.

Note that $u_1(t)$ and $-u_2(t)$ are different, contrarily to the case of even potentials. This asymmetry can be observed in figure 16. It corresponds to the

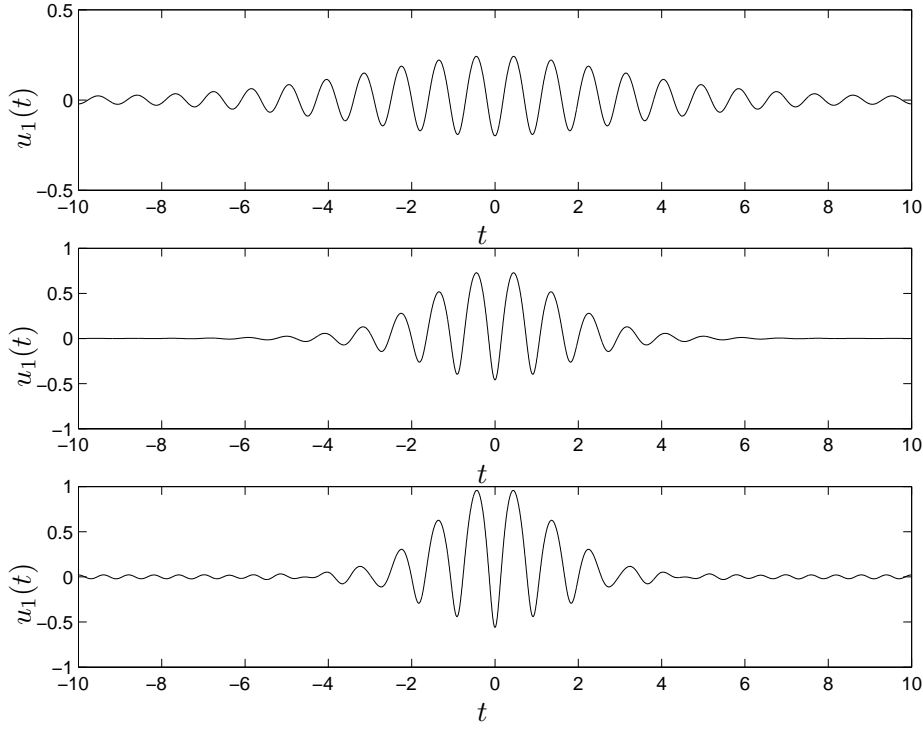


Figure 15: Localized numerical solutions of (5) for various propagation times T and the Morse potential $V(x) = \frac{1}{2}(1 - e^{-x})^2$. We plot $u_1(t)$ ($u_2(t)$ behaves similarly). One has $T = 6.7$, $T = 7.15$ and $T = 7.45$ from top to bottom, $(T_0, \gamma_0) \approx (6.63, 0.9) \in \Gamma_1$, $\gamma = \gamma_0$. The value of $\mu = T - T_0$ increases from top to bottom.

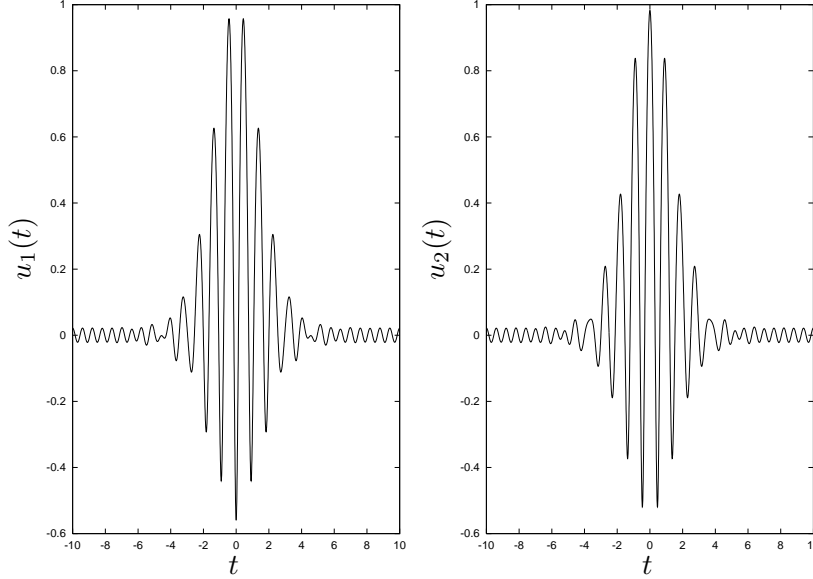


Figure 16: Localized numerical solution $(u_1(t), u_2(t))$ of (5) for $T = 7.45$ and the (asymmetric) Morse potential $V(x) = \frac{1}{2}(1 - e^{-x})^2$. One has $(T_0, \gamma_0) \approx (6.63, 0.9) \in \Gamma_1$, $\gamma = \gamma_0$. Note the difference between $u_1(t)$ and $-u_2(t)$.

fact that the symmetry $x_{n+1}(\tau) = -x_n(\tau - \frac{T}{2})$ is broken in the case of non even potentials.

In figure 17 we plot as a function of n the corresponding mass displacements $x_n(\tau)$, at times $\tau = 0$ and $\tau = T$ (we fix $T = 7.15$ in the left figure and $T = 7.45$ in the right one). As prescribed by condition (2), one recovers the same profile at both times, up to translation by 2 sites. One can note that neighboring oscillators are in phase near the breather center.

At $T = 7.15$ (figures 15, middle, and figure 17, left) no tail is visible at least at the figure scale. On the contrary a tail appears for $T = 7.45$ (figures 15, bottom, and figure 17, right).

Figure 18 provides a magnification of the tail of the solution profile. The oscillations observed near the boundary for $T = 6.9$ are not part of the solution tail and correspond in fact to oscillations of the central hump at a frequency close to q_0 (near this value of T the solution is weakly localized, see figure 15, top). The magnification shows small oscillations for $T = 7.15$ with a frequency close to the frequency observed for $T = 6.9$, therefore we attribute these oscillations to the damped central part of the solution, i.e. to the component $A(t)$ approximated by (24). Consequently we do not find for $T = 7.15$ a visible track of an oscillatory tail corresponding to components $C(t), D(t)$. On the contrary, in figure 18 a nondecaying tail with a frequency close to q_2 is clearly visible at $T = 7.45$ and

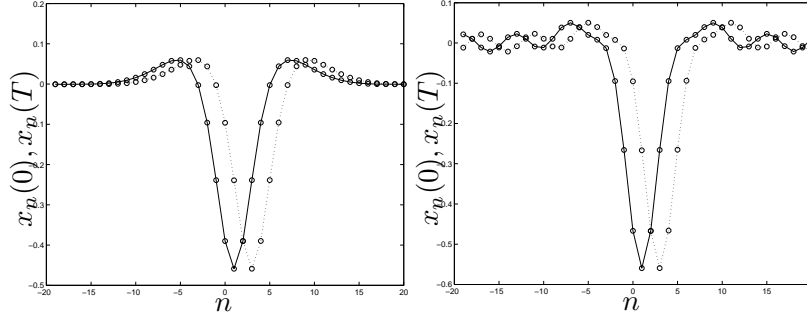


Figure 17: Numerical solution of (1)-(2) for $T = 7.15$ (left), $T = 7.45$ (right) and $p = 2$. We consider $V(x) = \frac{1}{2}(1 - e^{-x})^2$, $\gamma = \gamma_0 \approx 0.9$, $T_0 \approx 6.63$ ($(T_0, \gamma_0) \in \Gamma_1$). The solution is plotted as a function of n , for $\tau = 0$ (continuous line) and $\tau = T$ (dotted line). It corresponds via system (5) to profiles $u_1(t)$ in figure 15 (middle and bottom).

larger values of T (i.e. for larger values of μ). The nondecaying tail is also visible for some smaller values of T but the amplitude becomes very small (the tail size is decreased approximately by a factor of 100 for $T = 7.35$, see figure 18).

Figure 19 shows the Fourier spectrum of $u_1(t)$ for $T = 7.45$ and one can observe a sharp peak at a frequency close to $q_2/2\pi \approx 1.6$. The damped oscillations of the central hump (approximated by (24)) at a frequency close to q_0 appear as broad peaks and involve harmonics of all orders. In particular, figure 15 (bottom) clearly shows that the oscillatory part of the central hump has a nonzero time average. This situation contrasts with the even potential case (figure 7), in which these oscillations only involve odd order harmonics.

Another difference with respect to the even potential case is that solutions tails correspond here to the component D of (35) instead of C (the tail oscillates at a frequency close to q_2 instead of q_1). Consequently the oscillatory tail consists in a time-periodic travelling wave, instead of a time-periodic pulsating travelling wave as in (27). Note that we conjecture in fact the existence of a very small oscillatory component $C(t)$ (not visible in figure 16), which might be hidden in the broad peak of figure 19 close to $2q_0$ ($\frac{2q_0}{2\pi} \approx 2.22$ and $\frac{q_1}{2\pi} \approx 2.30$ are rather close). This is by analogy to the small amplitude regime described by the normal form (19). Indeed we conjecture that bifurcating homoclinic orbits of the full normal form have generically nonvanishing components C, D , except if T, γ satisfy two (one for each component) compatibility conditions ([28], section 5.3).

We end by a study of travelling breathers amplitude versus $\mu = T - T_0$ in the large amplitude regime (figure 20). One finds that the amplitude behaves approximately as μ^δ for relatively large values of μ (corresponding to highly localized solutions), with $\delta \approx 0.56$. A $\mu^{1/2}$ dependency of the amplitude (at leading order)

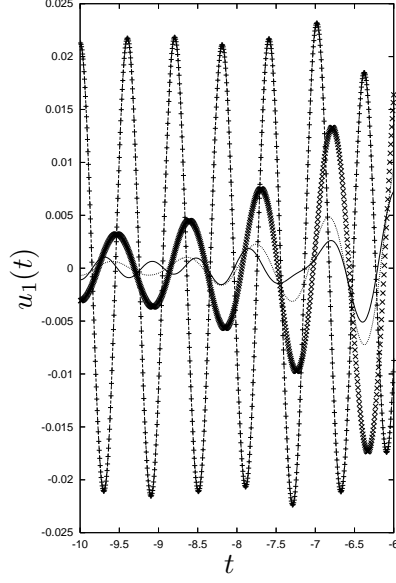


Figure 18: Magnification of the tail of localized solutions (component $u_1(t)$) for the Morse potential with $\gamma = \gamma_0 \approx 0.9$, $T_0 \approx 6.63$ ($(T_0, \gamma_0) \in \Gamma_1$). We consider several values of T : $T = 6.9$ (crosses \times), $T = 7.15$ (dashed line), $T = 7.35$ (continuous line), $T = 7.45$ (crosses $+$). The minimal tail size is found around $T = 7.15$. Cases $T = 7.15$ and $T = 7.45$ can be compared with figure 15.

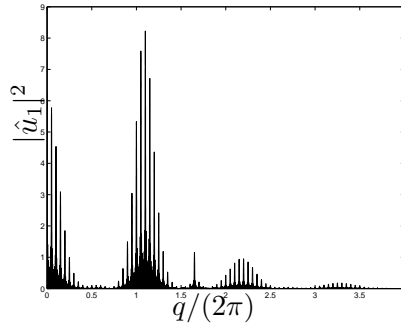


Figure 19: Fourier spectrum of $u_1(t)$ (the spectrum of $u_2(t)$ is similar) for $T = 7.45$, $\gamma = \gamma_0$, $(T_0, \gamma_0) \approx (6.63, 0.9) \in \Gamma_1$. The corresponding profile of figure 16 has been extended with periodic boundary conditions. Note the sharp frequency peak close to $\frac{q_2}{2\pi} \approx 1.6$. One has $\frac{q_0}{2\pi} \approx 1.11$, $\frac{q_1}{2\pi} \approx 2.30$.

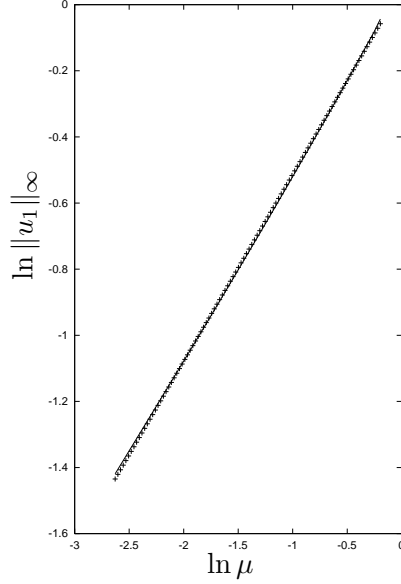


Figure 20: Maximal amplitude $\|u_1\|_\infty$ of a numerical solution of (5) (continuous line) as a function of μ , in logarithmic scales. The dotted line represents a linear regression. One has $V(x) = \frac{1}{2}(1 - e^{-x})^2$, $\gamma = \gamma_0 \approx 0.9$, $T_0 \approx 6.63$ ($(T_0, \gamma_0) \in \Gamma_1$), $\mu = T - T_0$. A similar behaviour is observed for $u_2(t)$.

is expected in the small amplitude regime $\mu \approx 0$ [28]. Surprisingly a rather similar behaviour is observed in the large amplitude regime. In addition the scaling in amplitude is rather similar to the case of equation (8) with a quartic interaction potential (section 3.2).

References

- [1] M.J. Ablowitz and J.F. Ladik. Nonlinear differential-difference equations and Fourier analysis, *J. Math. Phys.* 17, 1011-1018 (1976).
- [2] M.J. Ablowitz, Z. Musslimani and G. Biondini. Methods for discrete solitons in nonlinear lattices, *Phys. Rev. E* 65 (2002).
- [3] M.J. Ablowitz and Z. Musslimani. Discrete spatial solitons in a diffraction-managed nonlinear waveguide array : a unified approach, *Physica D* 184, 276-303 (2003).
- [4] A.A. Aigner, A.R. Champneys and V.M. Rothos. A new barrier to the existence of moving kinks in Frenkel-Kontorova lattices, *Physica D* 186, 148-170 (2003).

- [5] S. Aubry, T. Cr  t  gny. Mobility and reactivity of discrete breathers, *Physica D* 119, 34-46 (1998).
- [6] A. Berger, R.S. MacKay, V.M. Rothos. A criterion for non-persistence of travelling breathers for perturbations of the Ablowitz-Ladik lattice. *Discrete Cont. Dyn. Sys. B* 4, n. 4, 911-920 (2004).
- [7] S.R. Bickham, S.A. Kiselev and A.J. Sievers. Stationary and moving intrinsic localized modes in one-dimensional monoatomic lattices with cubic and quartic anharmonicity, *Phys. Rev. B* 47, 21 (1993).
- [8] A.R. Champneys. Codimension-one persistence beyond all orders of homoclinic orbits to singular saddle centres in reversible systems, *Nonlinearity* 14, 87-112 (2000).
- [9] D. Chen, S. Aubry, G.P. Tsironis. Breather mobility in discrete ϕ^4 lattices. *Phys. Rev. Lett.* 77, 4776 (1996).
- [10] J Cuevas, J.F.R. Archilla, Yu.B. Gaididei, F.R. Romero. Moving breathers in a DNA model with competing short- and long- range dispersive interactions, *Physica D* 163, 106-126 (2002).
- [11] J Cuevas, F. Palmero, J.F.R. Archilla, F.R. Romero. Moving discrete breathers in a Klein-Gordon chain with an impurity, *J. Phys. A : Math. Gen.* 35, 10519-10530 (2002).
- [12] T. Dauxois, M. Peyrard and A.R. Bishop. Dynamics and thermodynamics of a nonlinear model for DNA denaturation, *Phys Rev E* 47, n. 1, 684 (1993).
- [13] T. Dauxois, M. Peyrard and C.R. Willis. Discreteness effects on the formation and propagation of breathers in nonlinear Klein-Gordon equations, *Phys. Rev. E* 48, 4768 (1993).
- [14] D.B. Duncan, J.C. Eilbeck, H. Feddersen and J.A.D. Wattis. Solitons in lattices, *Physica D* 68, 1-11 (1993).
- [15] J.C. Eilbeck. Numerical simulations of the dynamics of polypeptide chains and proteins. In Chikao Kawabata and A.R. Bishop, editors, *Computer Analysis for Life Science - Progress and Challenges in Biological and Synthetic Polymer Research*, pages 12-21, Tokyo, 1986, Ohmsha.
- [16] J.C. Eilbeck and R. Flesch. Calculation of families of solitary waves on discrete lattices, *Physics Letters A* 149, 200-202 (1990).

- [17] H. Feddersen. Solitary wave solutions to the discrete nonlinear Shrödinger equation. In: M. Remoissenet and M. Peyrard, editors, *Nonlinear Coherent Structures in Physics and Biology*, Lecture Notes in Physics vol. 393 (Springer-Verlag, 1991), p. 159-167.
- [18] S. Flach and K. Kladko. Moving discrete breathers ?, *Physica D* 127, 61-72 (1999).
- [19] S. Flach and C.R. Willis. Movability of localized excitations in Nonlinear Discrete systems: a separatrix problem, *Phys. Rev. Lett.* 72, 1777 (1994).
- [20] S. Flach, Y. Zolotaryuk and K. Kladko. Moving kinks and pulses: an inverse method, *Phys. Rev. E* 59, 6105-6115 (1999).
- [21] S. Flach and C.R. Willis. Discrete Breathers, *Physics Reports* 295, 181-264 (1998).
- [22] D. Hennig, J.F.R. Archilla, J. Agarwal. Nonlinear charge transport mechanism in periodic and disordered DNA, *Physica D* 180, 256-272 (2003).
- [23] J.M. Hyman, D.W. McLaughlin and A.C. Scott. On Davydov's alpha-helix solitons, *Physica D* 3, 23-44 (1981).
- [24] G. Iooss, M. Adelmeyer. Topics in bifurcation theory and applications, *Adv. Ser. Nonlinear Dynamics* 3, World Sci. (1992).
- [25] G. Iooss, K. Kirchgässner. Travelling waves in a chain of coupled nonlinear oscillators, *Commun. Math. Phys.* 211, 439-464 (2000).
- [26] G. Iooss, E. Lombardi. Polynomial normal forms with exponentially small remainder for analytic vector fields. Preprint Institut Non Linéaire de Nice, 2004.
- [27] G. Iooss, M-C Pérouème. Perturbed homoclinic solutions in reversible 1:1 resonance vector fields, *J. Diff. Eqs.* 102, 62-88 (1993).
- [28] G. James, Y. Sire. Travelling breathers with exponentially small tails in a chain of nonlinear oscillators, to appear in *Comm. Math. Phys.* (2004). <http://www.gmm.insa-tlse.fr/~james/>
- [29] M. Kastner and J-A. Sepulchre. Effective Hamiltonian for traveling discrete breathers in the FPU chain. Submitted to *Discrete Cont. Dyn. Sys. B* (2003).
- [30] E. Lombardi. Phenomena beyond all orders and bifurcations of reversible homoclinic connections near higher resonances, *Lecture Notes in Mathematics*, Springer-Verlag, vol. 1741 (2000).

- [31] R.S. MacKay, S. Aubry. Proof of existence of breathers for time-reversible or Hamiltonian networks of weakly coupled oscillators, *Nonlinearity* 7 1623-1643 (1994).
- [32] R.S. MacKay, J-A. Sepulchre. Effective Hamiltonian for travelling discrete breathers, *J. Phys. A* 35, 3985-4002 (2002).
- [33] A.M. Morgante, M. Johansson, G. Kopidakis and S. Aubry. Standing wave instabilities in a chain of nonlinear coupled oscillators, *Physica D* 162, 53-94 (2002).
- [34] M.J.D. Powell. A hybrid method for nonlinear algebraic equations, in *Numerical Methods for Nonlinear Algebraic Equations*. Gordon and Breach (1970).
- [35] M. Peyrard, A.R. Bishop. Statistical Mechanics of a nonlinear model for DNA denaturation, *Phys. Rev. Lett.* 62, 2755 (1989).
- [36] M. Remoissenet. Low-amplitude breather and envelope solitons in quasi-one-dimensional physical models, *Phys. Rev. B* 33, number 4, 2386 (1986).
- [37] K.W. Sandusky, J.B. Page and K.E. Schmidt. Stability and motion of intrinsic localized modes in nonlinear periodic lattices, *Phys. Rev. B* 46, 10 (1992).
- [38] A.V. Savin, Y. Zolotaryuk, J.C. Eilbeck. Moving kinks and nanopterons in the nonlinear Klein-Gordon lattice, *Physica D* 138, 267-281 (2000).
- [39] A.C. Scott. *Nonlinear Science*, Oxford University Press, Oxford, 1999.
- [40] J-A. Sepulchre. Energy barriers in coupled oscillators: from discrete kinks to discrete breathers, *Proceedings of the Conference on Localization and Energy Transfer in Nonlinear Systems, June 17-21, 2002, San Lorenzo de El Escorial, Madrid, Spain; World Scientific*, Eds L. Vazquez, R.S. MacKay, M-P. Zorzano, 102-129 (2003).
- [41] Y. Sire, G. James. Travelling breathers in Klein-Gordon chains, *C. R. Acad. Sci. Paris, Ser. I* 338, 661-666 (2004).
- [42] Y. Sire. Travelling breathers in Klein-Gordon lattices as homoclinic orbits to p -tori, submitted to *J. Dyn. Diff. Eq.* (2004).
- [43] J. Szeftel, G. Huang and V. Konotop. On the existence of moving breathers in one-dimensional anharmonic lattices, *Physica D* 181, 215-221 (2003).

- [44] S. Takeno and K. Hori. A propagating self-localized mode in a one-dimensional lattice with quartic anharmonicity, *J. Phys. Soc. Japan* 59, 3037 (1990).
- [45] A.J. Sievers and S. Takeno. Intrinsic localized modes in anharmonic crystals, *Phys. Rev. Lett.* 61, 970-973 (1988).
- [46] J.L. Ting and M. Peyrard. Effective breather trapping mechanism for DNA transcription, *Phys. Rev. E* 53, 1011 (1996).
- [47] A. Vanderbauwhede, G. Iooss. Center manifold theory in infinite dimensions. *Dynamics reported 1*, new series, 125-163 (1992).